



Research Article

Green mediated synthesis of palladium nanoparticles using aqueous leaf extract of *Gymnema sylvestre* for catalytic reduction of Cr (VI)



J. Kadam¹ · S. Madiwale² · B. Bashte² · S. Dindorkar¹ · P. Dhawal² · P. More¹

Received: 17 May 2020 / Accepted: 12 October 2020 / Published online: 21 October 2020

© Springer Nature Switzerland AG 2020

Abstract

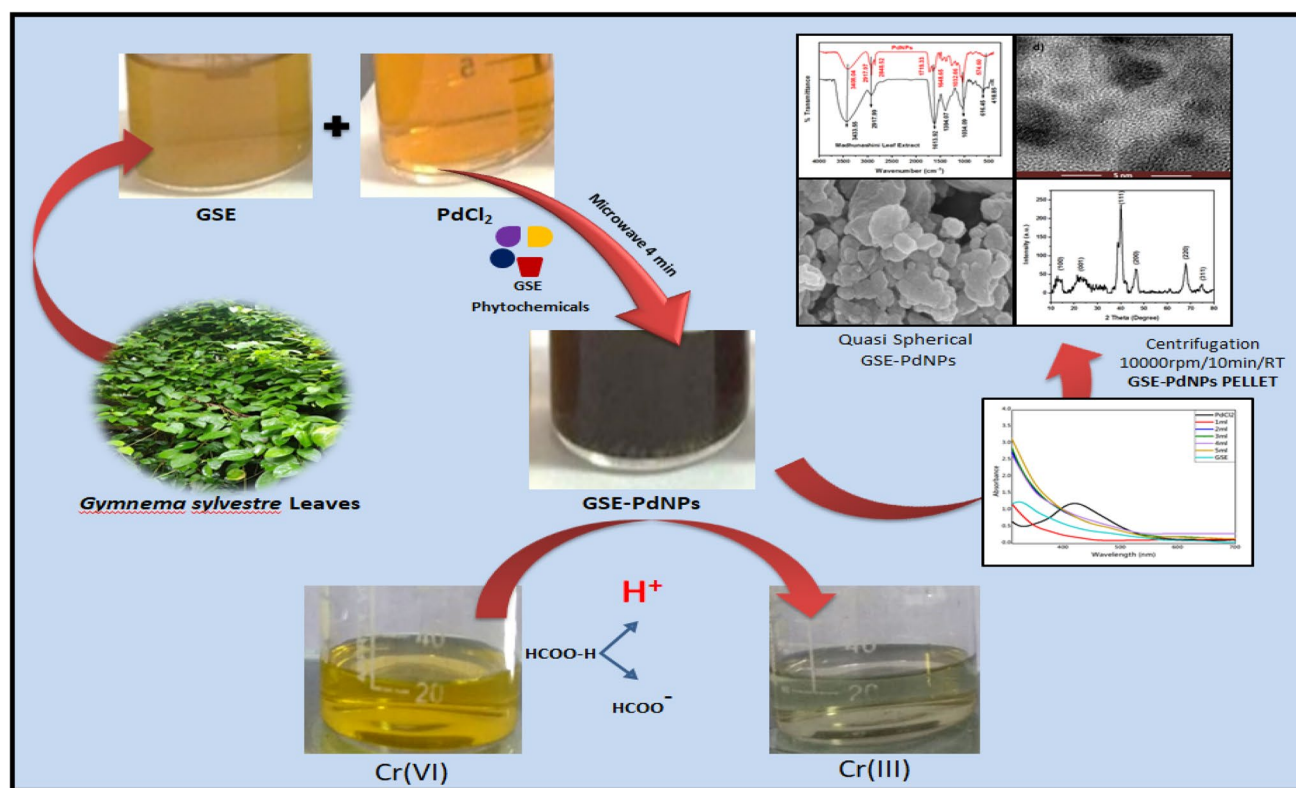
Palladium nanoparticles (PdNPs) were synthesised using a microwave technique using *Gymnema sylvestre* (GSE) leaf extract. PdNPs were tailored to different PdCl₂ and plant extract concentrations. Using XRD the crystalline existence of GSE-PdNPs has been established, confirming the formation of face-centered cubic structure. UV–Vis spectra of PdNPs confirmed the reduction of Pd²⁺ to Pd⁰. The FTIR spectra indicate the existence of functional groups which are responsible for nanoparticles reduction and progression. The SEM discloses quasi-sphere nanoparticles without agglomeration or aggregation which TEM confirms further. The reduction of Cr (VI) was performed with PdNPs (10 mg/L) and achieved a reduction of 96% within 30 min. In order to investigate the efficient reduction of chromium from Cr (VI) to Cr (III), different reaction system parameters have been optimised.

✉ P. More, paresh.m34@gmail.com | ¹Department of Chemistry, K.E.T's, Vinayak Ganesh Vaze College of Arts, Science and Commerce, Mithagar Road, Mulund (E), Mumbai, Maharashtra 400081, India. ²Animal Biotechnology and Biochemistry Division, Scientific Research Center, Vaze College Campus, Mithagar Road, Mulund (E), Mumbai, Maharashtra 400081, India.



SN Applied Sciences (2020) 2:1854 | <https://doi.org/10.1007/s42452-020-03663-5>

Graphic abstract



Keywords Green synthesis · *Gymnema sylvestre* · Palladium nanoparticles · Chromium reduction

1 Introduction

Heavy metals contamination has become a serious issue of concern around the world as it has gained impetus due to the increase in the use and processing of heavy metals during various activities. Amongst them, Cr (VI) is the most hazardous one. Cr (VI) has hazardous effects on organisms and its removal from soil and water bodies has gained a considerable attention in last few decades [1, 2]. Cr (VI) is known a highly toxic, non-biodegradable and cancer causing material. It has toxicity one hundred times higher than that of Cr (III) [3]. Various diseases such as lung cancer, dermatitis and nasopharynx are due to hexavalent chromium [4, 5]. Various methodologies have been employed by the researchers for removal of Cr (VI) from aqueous medium from last so many years.

The use of inorganic nanoparticles as reductants as well as catalysts for Cr (VI) reduction has become the subject of interest nowadays. This is due to high efficiency, low cost, environment friendly approach and applicability on industrial scale. Further no harmful by product is formed as compared to organic matter where re-oxidation may

occur [6]. In this treatment, Cr (VI) is completely converted into Cr (III) which has low mobility as compared to Cr (VI) [7]. Inorganic nanoparticles based materials used for Cr (VI) reduction may have some toxic effects on aquatic life. To avoid toxic effects some noble metals like Pt, Pd and Ag which do not have any significant toxic effects on aqueous environment are used. Thus, the conversion of toxic Cr (VI) to non-toxic Cr (III) represents a major remediation method for controlling chromium intoxication in the environment [8]. Palladium nanoparticles act as an excellent homogenous or heterogeneous catalyst [9] and have been explored intensively in catalytic hydrogenation reactions [10]. However, the high cost of preparation of heterogeneous catalysts restricts their applications, especially in large-scale process [11]. Reduction of Chromium (VI) using formic acid as an electron donor as well as in Suzuki–Miyaura coupling reaction was successfully studied using palladium nanoparticles [12, 13]. Conventional chemical methods for the productions of PdNPs often release toxic chemicals and require high pressure and temperature during synthesis process. Therefore, there is an urgent need to improve the technique which

can synthesize nanoparticles under ambient conditions using non-toxic reagents and solvents. The concept of green chemistry becomes more significant in such circumstances [14]. Additionally, this environment friendly procedure includes a simple reaction set up, mild reaction conditions, use of non-toxic medium such as water and microbes or plant extract [15]. Mahmoud Nasrollahzadeh et al. [16] reported reduction of Chromium (VI) using green synthesis of PdNPs using *Gardenia taitensis* leaf extract in the presence of NaBH_4 . Pankaj Das et al. reported reduction of Chromium (VI) using green synthesis of PdNPs *Garciniapedunculata* Roxb as bioreductant and starch (0.3%) as bio-stabilizer [17]. Mahmoud Nasrollahzadeh et al. [18] synthesized palladium/sodium borosilicate nanocomposite by using aqueous extract of the leaves of *Euphorbia milii* as bio-reducing and stabilizing agent. Herein we report the unique one-step environmentally benign synthesis of palladium nanoparticles using a leaf extract of *Gymnema sylvestre*. It involves synergistic reduction, stabilization and capping of the nanoparticles [19, 20]. *Gymnema sylvestre* commonly known as "Madhunashini/Gurmar", is distributed over most of India and has a reputation in traditional medicine as a stomachic, diuretic, and a remedy to control diabetes mellitus [21]. Use of GSE leaf extract in the synthesis of silver and gold nanoparticles has been reported [22, 23], however its use in synthesis of palladium nanoparticles has not been explored. The leaf extract of GSE contains phenolic compounds, flavonoids and tannins [24, 25] which may be responsible for the reduction and stabilization of metallic nanoparticles. Current research focuses on the green synthesis of palladium nanoparticles using GSE leaf extract and to investigate their catalytic efficiency towards maximum reduction of hexavalent chromium in the presence of minimal amount of reducing agent. The plausible mechanism of reduction of PdNPs as well as the reduction of Cr (VI) to Cr (III) is discussed in detail.

2 Materials and methods

2.1 Chemicals

AR grade Palladium chloride (PdCl_2) and HCOOH were procured from Sigma Aldrich, $\text{K}_2\text{Cr}_2\text{O}_7$ from S. D. Fine and *G. sylvestre* leaves were taken from the plant grown in the premises of V. G. Vaze College (Mulund).

2.2 Preparation of *Gymnema sylvestre* leaves extract (GSE)

Freshly collected leaves of *G. sylvestre* were thoroughly washed with distilled water to remove any surface debris and then shade dried at room temperature. Leaves were

ground in the mortar and pestle. 10 g of powdered leaves were extracted with 100 mL of deionised water and was heated to 70 °C for 5 min. The mixture was filtered through muslin cloth followed by Whatmann filter paper no.1. This extract (GSE) was kept in the sterile bottles and stored at 3–5 °C for further use.

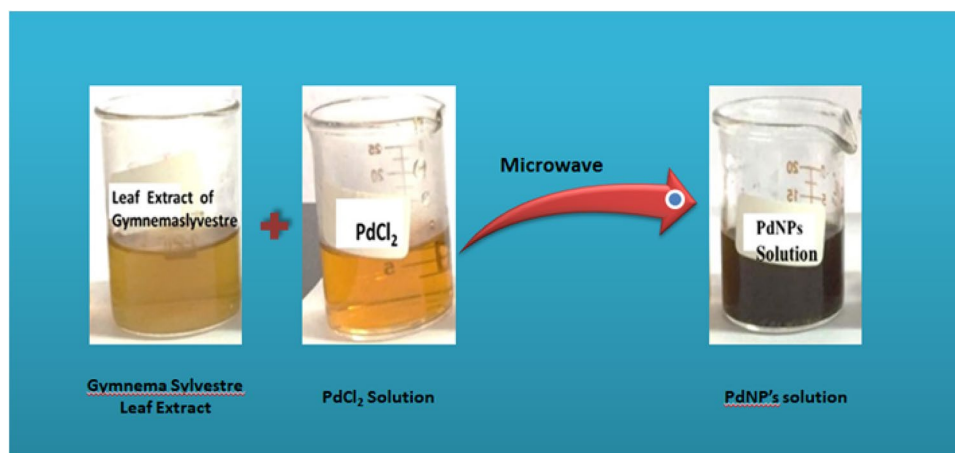
2.3 Synthesis of palladium nanoparticles (GSE-PdNPs) using GSE

The reactor used for the synthesis of PdNPs was 100 mL Pyrex beaker. A reaction system of 10 mL was set up for the synthesis of PdNPs. To the varying GSE volumes (1, 2, 3, 4, and 5 mL) prepared in de-ionised distilled water in the absence of any other external reducing agent, required amount of PdCl_2 was added. The mixture was placed in the microwave of 350 W for 5 min. The reaction was monitored for change in optical properties from yellow colour to dark brown, consistent with the formation of PdNPs [26]. Appearance of precipitate with time was observed within 5 min upon heating the reaction mixture of GSE and PdCl_2 in microwave, which indicates formation of GSE-PdNPs as depicted in Fig. 1. The as-synthesized GSE-PdNPs were purified by carrying out centrifugation at 10,000 rpm for 10 min. The pellet obtained was further purified with deionised water to remove residues of any un-reacted GSE. Purified PdNPs were dried overnight and were used for further characterization and catalytic application [27].

2.4 Characterization of GSE-PdNPs

Powder XRD pattern of purified GSE-PdNPs was recorded using X-ray diffractometer (Philips PAN analytical with Cu K α radiation, $\lambda = 1.5418$) in order to study the crystalline structure of purified GSE-PdNPs. As-synthesized GSE-PdNPs were screened for its optical properties using UV-visible spectrophotometer (model 1800 Shimadzu Japan) over wavelength range from 300 to 700 nm. Fourier Transform Infra-Red (FTIR) was performed to identify possible biological compounds present in GSE and role of those compounds as reducing and capping agents in purified GSE-PdNPs by using 3000 Hyperion Microscope with vertex 80 FTIR. The microstructure, sample morphology and elemental mapping (EDAX) of purified GSE-PdNPs was characterized by JEOL JSM-7600 F, FEG-SEM. Transmission electron microscopy (TEM), selected area diffraction pattern (SAED) and EDS elemental mapping using field emission gun-TEM 300 kV was performed for understanding morphology, size and elemental composition of purified GSE-PdNPs. Catalytic activities of GSE-PdNPs were monitored using UV-visible spectrophotometer.

Fig. 1 Color formation of GSE-PdNPs



2.5 Reduction of Cr (VI) using GSE-PdNPs catalyst

Experiments were performed to analyse the catalytic conversion of toxic Cr (VI) to nontoxic Cr (III) state using formic acid (HCOOH) as a reducing agent, biosynthesized GSE-PdNPs as a catalyst and $K_2Cr_2O_7$ as a precursor of Cr (VI). Catalytic efficiency of GSE-PdNPs was optimized by studying the effect of various influencing factors such as quantity of HCOOH [1%, 1.25%, 5%], initial concentration of Cr (VI) [100 mg/L, 150 mg/L and 200 mg/L] and dosage of GSE-PdNPs [1 mg/L, 5 mg/L and 10 mg/L] for reduction of Cr (VI) to Cr (III) in the aqueous solution. A typical reaction system consisted of 25 mL of $K_2Cr_2O_7$ solution prepared in deionised water, HCOOH and GSE-PdNPs. The reaction system was maintained at room temperature without stirring, throughout the experiment. At time interval of 15 min, 3 mL aliquot was withdrawn from the system and was subjected to UV–visible spectrophotometric analysis, in the range of 200–600 nm. Control system, without GSE-PdNPs was also maintained. Absorbance of Cr (VI) in both, test and the control systems was measured at 350 nm (λ_{max} of Cr (VI)) at respective time interval for upto 120 min. These absorbance values were later used for calculating percent reduction by using following formula;

$$\% \text{Reduction} = \frac{C_0 - C_t}{C_0} \times 100$$

where, C_0 is the initial Cr (VI) concentration and C_t is the concentration of Cr (VI) at time t . Graph of $\ln(C/C_0)$ versus time (min) was plotted to obtain linear regression for every reaction system and was used to calculate the kinetic parameters, such as, rate constant (k) in min^{-1} , Half-life $t_{(1/2)}$ in min and R^2 value.

3 Results and discussion

3.1 X-ray diffraction (XRD) analysis

The crystalline structure of GSE-PdNPs was determined by analysis of the obtained XRD pattern. Figure 2 revealed the well-defined characteristic diffraction peaks at 40.12° , 46.88° , 67.86° , 74.76° and 79.64° , respectively indexed to reflections from (111), (200), (220), (311) and (222). These obtained reflections demarcate the formation of face-centred cubic (fcc) lattice system of PdNPs (JCPDS card no. 87-0641). Intense reflection at (111) in contrast with the other four reflections explains (111) lattice plane is the favoured orientation for the biosynthesized PdNPs [28]. On the basis of full width at half maximum of the (111) reflection, the average crystallite size (~ 40 nm) of the PdNPs was determined using the Scherrer equation $D = (0.9\lambda/\beta\cos\theta)$ [29]. Two additional diffraction peaks at 14.44° (100) and 21.25° (001) were observed which can be attributed to the formation of PdO (JCPDS card no. 72-0200). Pd (0) formed might have got transformed into PdO due to aerial oxidation [30].

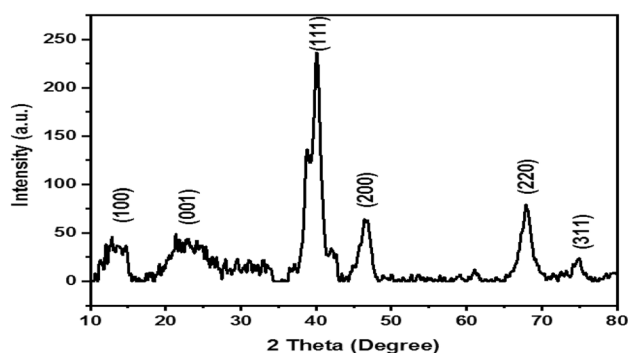


Fig. 2 XRD-analysis of GSE-PdNPs

3.2 UV-visible studies of GSE-PdNPs

Synthesis of GSE-PdNPs was monitored using UV-visible spectrophotometer. Factors such as, initial PdCl₂ concentration and leaf extract volume were studied for their influence on formation of PdNPs. PdCl₂ gave an intense peak at 425 nm due to presence of Pd (II) ions which was completely disappeared and replaced by broad and continuous absorption with increase in Surface Plasmon Resonance at 350–400 nm [31]. This clearly marked the conversion of Pd (II) ions to Pd (0) NPs. Also GSE alone did not show any peak at 425 nm indicating that the plant extract is free from interference of phytochemicals at 425 nm. As the reaction was performed at high temperature in the microwave oven, the nucleation initiated quickly and most of the Pd (II) was converted to Pd (0) during five minutes of the reaction. Optimization of PdCl₂ concentration and volume of GSE was performed to obtain standardised concentration of GSE and Pd (II) towards formation of GSE-PdNPs (Fig. 3a, b). Finally, the synthesis was conducted using optimized concentrations of 2 mL of GSE with 2 mM PdCl₂.

3.3 FTIR analysis of GSE-PdNPs

GSE and biosynthesized GSE-PdNPs were scanned in the range of 400–4000 cm⁻¹ by FTIR. It identifies the functional group of biomolecules present, that may have acted as possible reducing and capping agents in conversion of Pd²⁺ to Pd⁰. The FTIR spectra of GSE (Fig. 4) exhibited prominent absorption peaks at 3433.55 cm⁻¹, 2917.99 cm⁻¹, 1613.92 cm⁻¹, 1394.07 cm⁻¹, 1034.09 cm⁻¹ and 616.45 cm⁻¹, 418.85 cm⁻¹. Strong peak at 3433.55 cm⁻¹ corresponds to symmetrical stretching vibrations of –OH

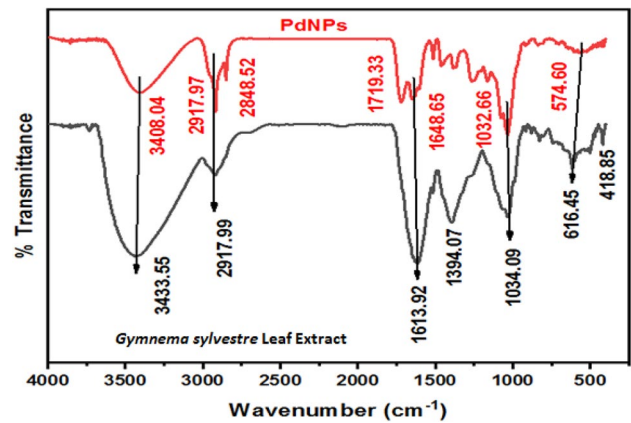


Fig. 4 FTIR spectra of plant extract and GSE-PdNPs

groups of hydroxyl molecules [32]. Absorption peaks at 2917.99 cm⁻¹ corresponds to C–H bond stretching. Band at 1613.92 cm⁻¹ can be ascribed to O–H deformation of water adsorbed on the surface of sample or C=O stretching vibrations [33]. The band at 1394.07 cm⁻¹ corresponds to Carbonyl stretching [34]. Absorption peak at 1034.09 cm⁻¹ may be attributed to ether linkages suggesting the presence of flavanones adsorbed on the surface of synthesized nanoparticles and band at 1034.09 cm⁻¹ may correspond to C–N stretching vibration of aromatic and aliphatic amines which can be attributed to the presence of complex phenolic compounds [35–37]

In comparison, the FTIR spectrum of purified GSE-PdNPs (Fig. 4) exhibited marginal peak shift and lower absorption band intensities at 3408.04 cm⁻¹, 2917.97 cm⁻¹, 1719.33 cm⁻¹, 1648.65 cm⁻¹, 1032.66 cm⁻¹ and 1032.66 cm⁻¹; this decrease in intensities

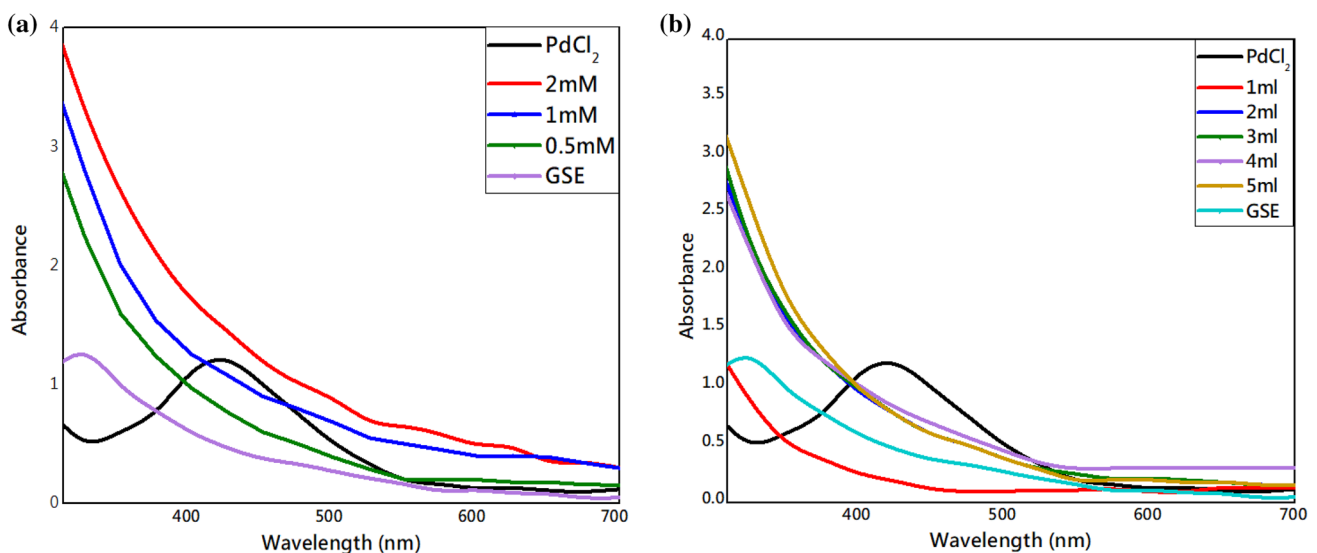


Fig. 3 UV-visible spectra at varying concentration of PdCl₂ **a** 0.5, 1, and 2 mM, **b** 1–5 mL

may suggest the involvement of hydroxyl, carbonyl and amine functional groups in fabrication of nanoparticles. It also revealed additional low intensity peaks at 2848.52 cm^{-1} , 1719.33 cm^{-1} , and 1385 cm^{-1} that may correspond to $-\text{CH}_2$ vibrations of aliphatic hydrocarbons [38], carboxyl groups from dimerised saturated aliphatic acids [39] and $\text{C}=\text{C}$ aromatic ring stretching vibrations, respectively. Based on the above FTIR analysis it can be predicted that phytoconstituents such as, phenolic compounds, flavanones, tannins, and aliphatic acids present in GSE may be involved in green synthesis of GSE-PdNPs.

The possible mechanism for the synthesis of PdNPs using GSE involves two steps (Fig. 5). Initially Pd(II) will undergo complexation with hydroxyl and carbonyl functional groups of various phytochemicals present in GSE. Due to the strong antioxidant nature and high reducing capacity, these hydroxyl and carbonyl functions will reduce Pd(II) to Pd(0) atoms and undergo oxidation to carboxyl groups. Pd atoms serve as nucleation sites for the growth of PdNPs. Finally, the size control and stabilization of PdNPs was achieved by the surface coating of these phytochemicals through binding interactions between metal atoms and oxygen containing functional groups [40].

3.4 SEM and EDAX analysis

Surface morphology and shape of GSE-PdNPs was examined using Scanning Electron Microscopy (SEM) technique as depicted in the Fig. 6. Purified GSE-PdNPs exhibited a homogeneous dispersion and lesser or no agglomeration [41]. Micrographs revealed that the synthesized nanoparticles are of nano-size and are quasi spherical, with an average diameter of $70 \pm 20\text{ nm}$. EDAX analysis confirmed the main component, elemental palladium (Fig. 6) and other elements such as C, O, S, Cl were observed may be due to the presence of traces of GSE.

3.5 TEM, SAED pattern analysis and EDS elemental mapping

FETEM was used to conduct the microstructural investigation of PdNPs (Fig. 7A). This revealed a spherical morphology that clearly displayed the various sizes of spheres (Fig. 7A: a, b). The TEM findings obtained were well in line with the SEM findings. The higher the number of spheres with an average diameter of 10–20 nm, but some of the spheres are wide (Fig. 7A: b). Figure 7A: c shows the different lattice fringes which corresponds to the (111), (200), (220), (311) lattice planes of PdNPs. The SAED pattern clearly shows the crystalline nature of the PdNPs (Fig. 7A: d). The lattice planes shown in TEM results were also consistent with XRD results. EDS elemental mapping image

Fig. 5 Plausible mechanism of reduction of Pd^{2+} to Pd^0 by flavonoids present in *Gymnema sylvestre* leaf extract to give GSE-PdNPs

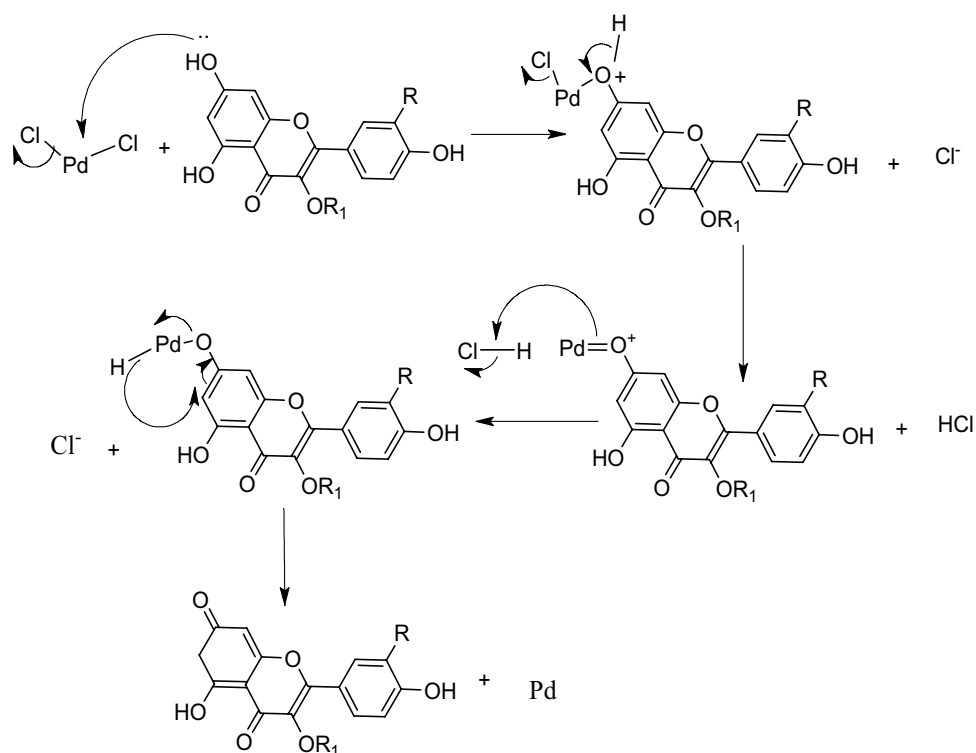
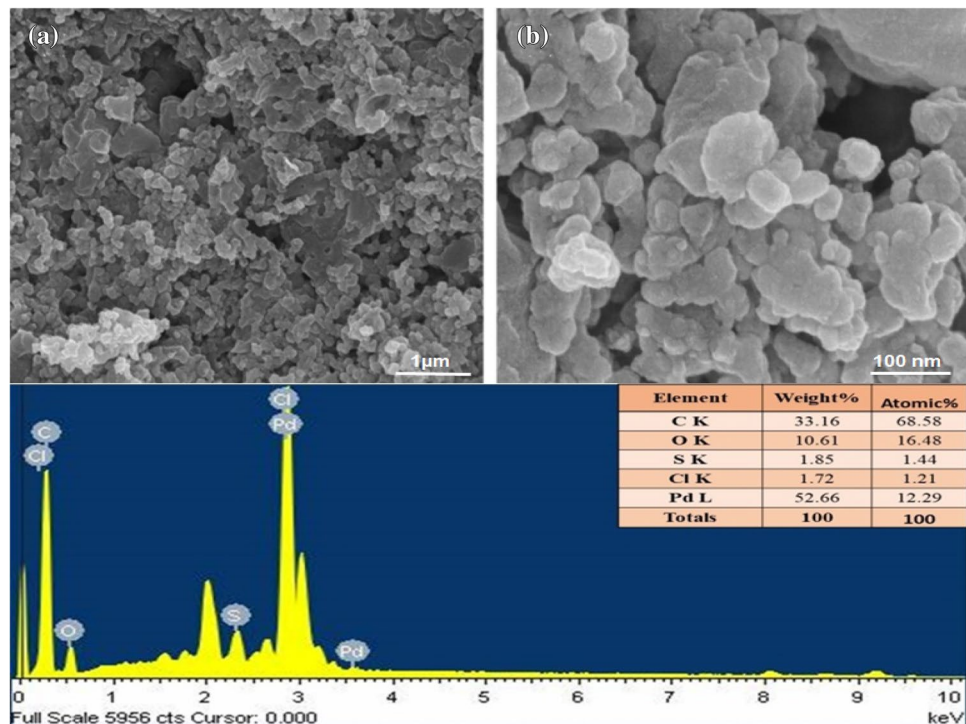


Fig. 6 SEM–EDX analysis of GSE-PdNPs

of GSE-PdNPs reveal the features as can be seen in Fig. 7B. The elemental profile detected the presence of Carbon, followed by palladium and other elements such as oxygen, chlorine and sulphur further confirms the data obtained in EDAX analysis. High proportion of carbon along with Cl, O and S might have resulted from the rich organic profile of GSE leaf extract. As mentioned earlier, FTIR spectra of plant extract and GSE-PdNPs functional groups such as carbonyl and hydroxyl from vivid phytochemicals such as flavonones, amines, aliphatic hydrocarbons have shown involvement in the bio-reduction of Pd^{2+} to Pd^0 . The EDS map hence shows the presence of additional elements which may be bound to the surface of Pd nanoparticles as reducing and capping agents.

3.6 Reduction of Cr^{+6} using GSE-PdNPs

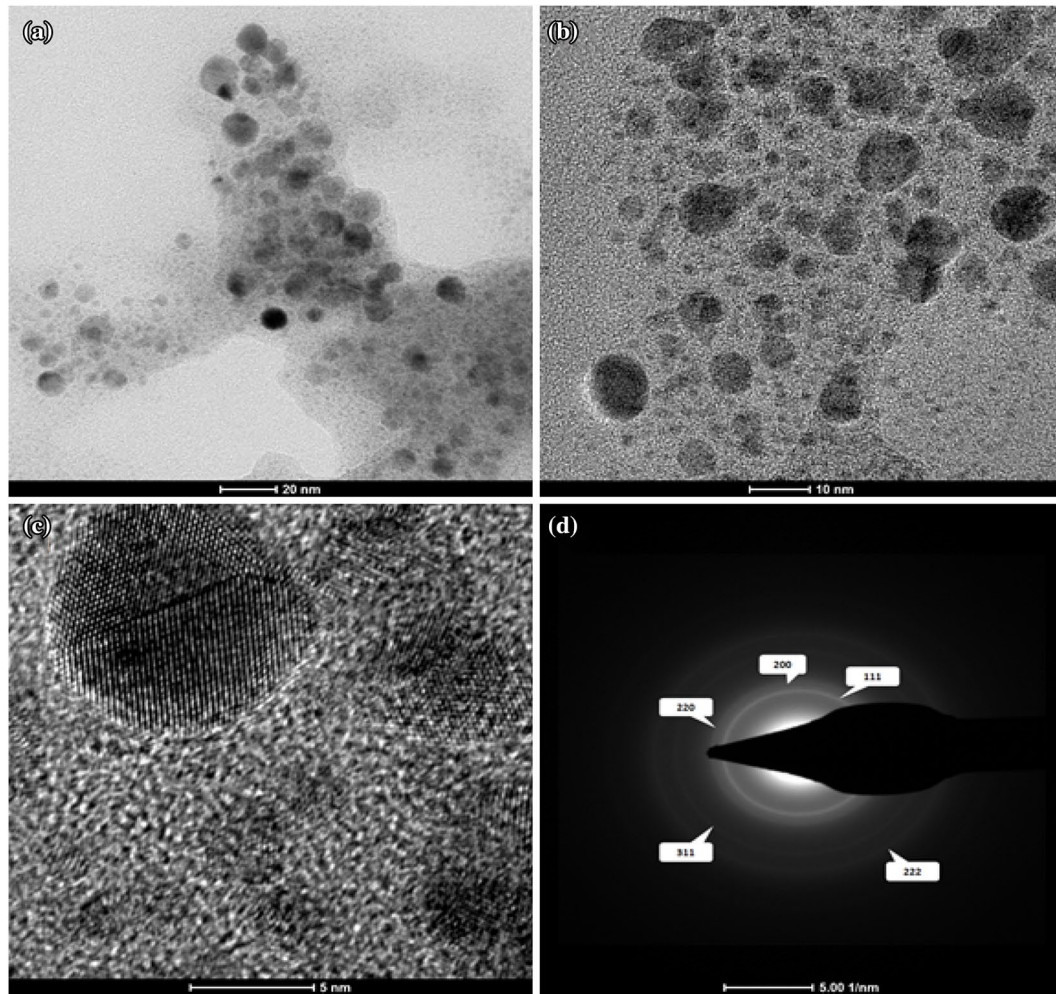
The catalytic activity of synthesized GSE-PdNPs was investigated for the reduction of Cr (VI) in the aqueous solution using formic acid as the reducing agent. Cr (VI) in the form of Potassium dichromate ($\text{K}_2\text{Cr}_2\text{O}_7$) was used. The addition of GSE-PdNPs exhibited catalytic performances for the reduction of Cr (VI) in the presence of minimum volume of formic acid. Reaction progress was monitored using UV–visible absorption spectroscopy. The absorption of Cr (VI) at 350 nm decreased along with the change in colour from yellow to colourless, with time, indicating the transition of Cr(VI) to Cr(III). This was further confirmed by the addition of excess of NaOH

to the final solution. The colour of solution changed to green after addition of excess NaOH because of the formation of hexahydroxochromate (III), which clearly gives the evidence for the presence of Cr (III) [42]. Cr (III) is the reduced form of Cr(VI) and less toxic in nature. For comparison, reduction of Cr(VI) to Cr(III) using only formic acid as a reducing agent (i.e., without the catalyst) was also carried out and it was observed that even after 120 min of reaction time it showed no efficient spectral shift. This result clearly suggests that the presence of GS-PdNPs-catalyst was mandatory to achieve Cr (VI) reduction.

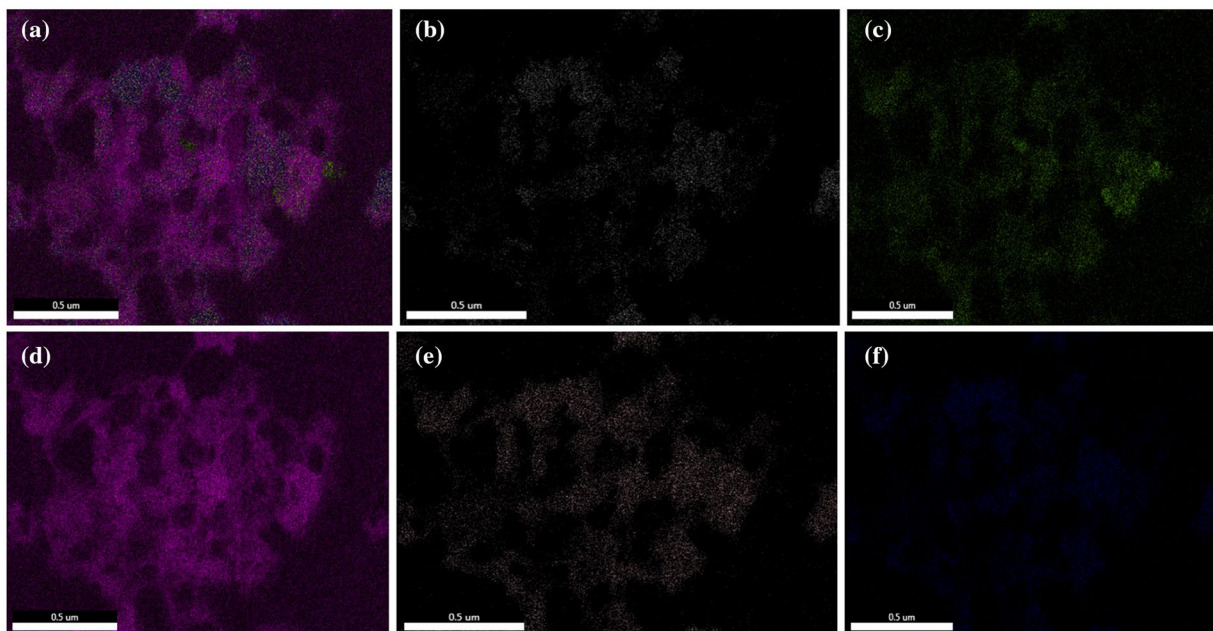
3.7 Effect of different parameters on chromium reduction

Major factor known to influence the catalytic reduction of chromium including dosage of formic acid, amount of GSE-PdNPs and initial concentration of Cr (VI) were each studied. Kinetic parameters (K in min^{-1} and $T_{1/2}$ in min) and correlation coefficients (R^2) for Cr (VI) for different systems are given in Table.1. Linear regression of $\ln(C/C_0)$ (where, C_t = Concentration of Cr (VI) at time 't' (min) and C_0 = Concentration of Cr (VI) at time 0 min) was estimated for every reaction and for every system pseudo first order nature of chromium reduction by GSE-PdNPs was confirmed.

A



B



◀**Fig. 7 A: a, b** TEM images, **c** a HRTEM image and **d** the SAED pattern palladium nanoparticles. **B:** Elemental mapping images, where **a** mixed, **b** palladium, **c** oxygen, **d** carbon, **e** chlorine and **f** sulphur of Pd nanoparticles

3.7.1 Varying concentration of formic acid

Formic acid is known to possess strong reducing properties and undergoes direct mineralization to carbon dioxide and hydrogen, in the presence of metal catalysts without the formation of intermediates, thereby attracting considerable interest as an agent in Cr(VI) reduction. Studies have shown that the performance of formic acid as a reducing agent could be improved via catalysis [42]. In the present study, three different concentrations, 1%, 1.25%, and 5% of formic acid were used, with 150 mg/L of $K_2Cr_2O_7$ solution and 10 mg/L of GSE-PdNPs constant, to evaluate the optimum dosage of formic acid in reduction of chromium Cr (VI). It was observed that Cr(VI) peak at 350 nm gradually decreased as the reaction time proceed. Figure 8a shows $\ln(C/C_0)$ versus time (in min) at varying concentration of formic acid. Quick reduction by 96% in 30 min was obtained with 1.25% of formic acid. Reaction systems, with 1% of formic acid demonstrated similar trend in reduction efficiency, however the time required was 75 min. 5% of formic acid lead to very slow i.e. 30.75% reduction efficiency in 120 min. Thus it was observed that the increase or decrease in the dosage of formic acid for fixed concentration of chromium alters the reducing efficiency. The decrease in the chromium reduction capability with 1% and 5% of formic acid may be attributed to the interference of in-situ formation of H^+ ions. The rate constant was found to be highest with 1.25% concentration of formic acid as depicted in the Table 1.

3.7.2 Varying concentration of GSE-PdNPs

GSE-PdNPs were varied as 10 mg/L, 5 mg/L and 1 mg/L, with constant 150 mg/L, $K_2Cr_2O_7$ and 1.25% formic acid. Negligible change in the peak intensity of Cr(VI) was observed for the system with 1 mg/L of PdNPs. Reduction up to 99.3% in 45 min and 75% in 120 min was observed spectrophotometrically for 10 mg/L and 5 mg/L reaction system respectively. $\ln(C/C_0)$ versus time in minutes at varying concentration of GSE-PdNPs is depicted in the Fig. 8b. These observations suggest that as the concentration of GSE-PdNPs increases, the time taken for reduction of chromium decreases. These can simply be attributed to greater concentration of available active sites resulting directly from the increased catalyst loading. The rate constant was found to be highest with the increase in the concentration as depicted in the Table 1.

3.7.3 Varying initial concentration of chromium

The standardization of Cr (VI) concentration in the system was studied for 100 mg/L, 150 mg/L and 200 mg/L of $K_2Cr_2O_7$ as the Cr (VI) representative. Concentration of GSE-PdNPs and formic acid were kept constant, i.e. 10 mg/L of GSE-PdNPs and 1.25% formic acid. The percentage reduction obtained were 94.37% and 98.27% for 100 mg/L and 200 mg/L concentration respectively after 60 min. However, faster reduction was observed with 150 mg/L showing 96% reduction in 30 min and $\approx 100\%$ was observed at the end of 45 min. $\ln(C/C_0)$ versus time in minute at varying concentration of Cr(VI) is depicted in the Fig. 8c. The rate constant was found to be highest with 150 mg/L concentration of $K_2Cr_2O_7$ as depicted in the Table 1.

A summary of reaction kinetic parameters is given in Table 1. Therefore, from the optimization studies of Cr(VI) reduction it was found that, 1.25% of formic acid, 150 mg/L of Cr(VI) and 10 mg/L of GSE-PdNPs is the optimized condition for reduction as $T_{(1/2)}$ calculated was least i.e. 4.31–4.9 min. pH plays a very vital role in the reduction of Cr (VI) to Cr (III), where the low pH could promote the electron transfer between GSE-PdNPs and chromium (VI). The efficiency of chromium reduction was very low at higher pH; this may be due to the fact that there is competition of hydroxyl ion (OH^-) with the chromium (VI) for adsorption sites. Further Cr (VI) is favourably adsorbed at lower pH values [43]. Reports suggest that reduction is favoured in acidic condition (pH=2). In the current study, pH of the resultant optimised reaction system was already 1.65 and hence pH alterations were not made [44]. UV-Vis Spectra representing Cr (VI) reduction using the optimized parameters is shown in Fig. 9. Titanium oxide and iron nanoparticles showed catalytic properties towards reduction Cr(VI) to Cr(III). However, after doping them with palladium their catalytic property enhanced many fold suggesting palladium increased catalytic potency of iron and TiO_2 . More notably, the Cr (VI) reduction obtained for GSE-PdNPs is far higher as compared to the previous studies (Table 2) [2, 11, 12, 19, 45–55].

3.7.4 Possible mechanism for Cr(VI) reduction

The catalytic efficiency of GSE-PdNPs was evaluated at room temperature for the reduction of highly toxic Cr (VI) to Cr (III). It was observed that in the presence of PdNPs the absorption peak of Cr (VI) decrease rapidly with time. The possible mechanism is discussed as per the below equations. the H^+ ions from formic acid and Cr (VI) ions from $K_2Cr_2O_7$ may get adsorbed (*ad) on the surface of nanoparticles and that may employ reduction of Cr(VI) to Cr(III).

Table 1 Summary of kinetics ($k \text{ min}^{-1}$ and $T_{1/2} \text{ min}$) and Correlation Constant for Cr(VI) reduction using green synthesis GSE-PdNPSs

System	Concentration	$k \text{ (min}^{-1}\text{)}$ from graph	$T_{1/2}$ (min) = $\ln(0.5)/k$	R^2 from graph
<i>Varying concentration of formic acid</i>				
150 mg/L Cr(VI)	1%	0.0677	10.39	0.8232
10 mg/L GSE-PdNPS	1.25%	0.1413	4.905	0.9618
	5%	0.004	169.0	0.8150
<i>Varying concentration of GSE-PdNPSs</i>				
150 mg/L Cr(VI)	1 mg/L	0.0003	2310	0.8879
1.25% formic acid	5 mg/L	0.0132	52.11	0.9729
	10 mg/L	0.1427	4.857	0.9712
<i>Varying concentration of Cr(VI)</i>				
10 mg/L GSE-PdNPS	100 mg/L	0.1173	5.909	0.9493
1.25% formic acid	150 mg/L	0.1564	4.431	0.9586
	200 mg/L	0.1179	5.879	0.9093
Control for standard system	150 mg/mL Cr (VI) 1.25% formic acid	0.0003	2310	0.8479

Bold values are the optimized conditions

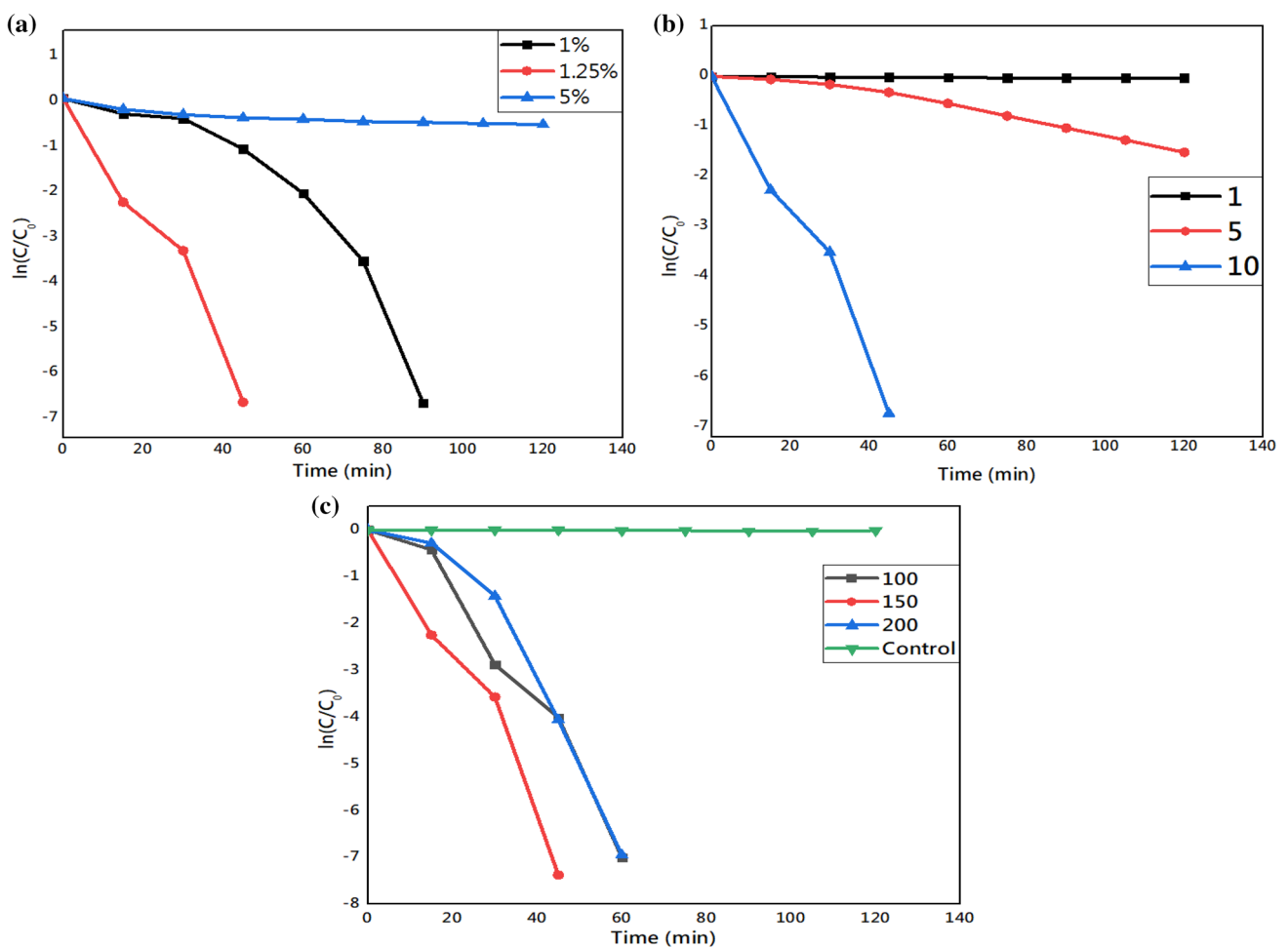


Fig. 8 a. $\ln(C/C_0)$ versus time taken for reduction of Cr (VI) at varying concentration of **a** formic acid (1%, 1.25 and 5%), **b** GSE-PdNPS (1 mg/L, 5 mg/L and 10 mg/L), **c** concentration of Cr(VI) (100 mg/L, 150 mg/L and 200 mg/L)

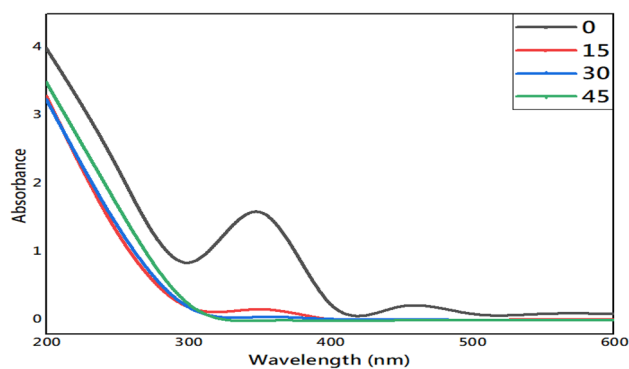


Fig. 9 Standardised system for reduction of Cr(VI) with 10 mg/L of GSE-PdNPs, 1.25% formic acid and 150 mg/L of Cr(VI)

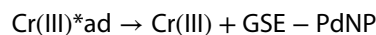
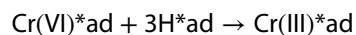
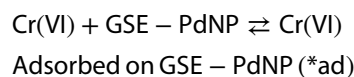
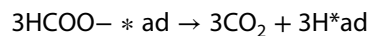


Table 2 Comparison of studies for Cr(VI) reduction using metal nanoparticles with present study

Metal nanoparticles	Reductant for NP synthesis	Cr(VI) (mg/L)	NP (mg/L)	Formic acid (ml/L)	Temperature/ conditions	Time (min)	Reduction percent	References
Sulfur	<i>Ficus benghalensis</i>	200	10	20.6	N.D	80	88.7%	[47]
Iron	Chemical synthesis starch	20	400	–	N.D	60	98%	[48]
Iron	<i>Eucalyptus</i> leaf extracts	10	1400	–	30 °C	35	98.9%	[49]
Titanium oxide	Chemical synthesis	50	1000	–	Sunlight	60	90%	[50]
Titanium oxide	Sol gel method	50	1000	–	Solar simulator	Monitored for 120	–	[51]
Fe–Ti oxide	Chemical synthesis	10	2000	–	UV irradiation RT	360	97.7%	[52]
Fe ₃ O ₄ /Pd@NeC	Chemical synthesis	588.36	1000	20	45 °C	3	100%	[53]
Bimetallic CuBiOS catalyst	Chemical synthesis	50	50	–	Dark 200 mg/L of NaBH ₄	20	99.7%	[54]
Bare palladium	<i>Shewanella loihica PV-4</i>	147.09	500	0.5	30 °C	180	100%	[2]
Immobilized palladium	Procyanidin-grafted egg-shell membrane	534.41	1363	73	44.85 °C	26	100%	[55]
Pd/Fe ₃ O ₄	<i>Hibiscus tiliaceus</i> L.	1000	400	40	50 °C	35	100%	[19]
Pd/sodium borosilicate	<i>Euphorbia milii</i> extract	1000	200	40	RT NaBH ₄	15	100%	[11]
Palladium	Nanofibrous mat PEI/PVA	338.30	46.93	30.6	50 °C	12	99.7%	[56]
Pd NPs/fTiO ₂	Chemical synthesis	588.36	300	17.32	30 °C	2.5	100%	[57]
Bare palladium starch as reductant	<i>Garcinia Pedunculata</i> Roxb	294.18	60	15	N.D	40	100%	[12]
Bare palladium No reductant added	<i>Gymnema sylvestre</i>	150	10	12	Dark RT	30	96%	Present study

Key: N.D temperature not defined, RT room temperature

4 Conclusion

In Summary, GSE-PdNPs were synthesized using aqueous leaf extract of *G. sylvestre*, by green approach. Bio-synthesized GSE-PdNPs were employed for the degradation of the toxic pollutant Cr (VI) into a non-toxic Cr (III) form. The green and simple method of synthesis, eco-friendly nature of the catalyst, very economical and excellent catalytic activities, these properties made GSE-PdNPs a perfect candidate for the large scale Cr (VI) effluent treatment.

Acknowledgement The authors would like to thank SAIF IIT Bombay for conducting FTIR, TEM, SEM and EDAX of our samples. We would also like to thank Mr. Nilesh Kulkarni Tata Institute of Fundamental Research for performing XRD analysis.

Compliance with ethical standards

Conflict of interest The authors declare no conflict of interest.

References

- Zhou X, Jing G, Lv B, Zhou Z, Zhu R (2016) Highly efficient removal of chromium (VI) by Fe/Ni bimetallic nanoparticles in an ultrasound-assisted system. *Chemosphere* 160:332–341
- Veerakumar P, Thanasekaran P, Lin KC, Liu SB (2017) Biomass derived sheet-like carbon/palladium nanocomposite: an excellent opportunity for reduction of toxic hexavalent chromium. *ACS Sustain ChemEng* 5(6):5302–5312
- Yang GC, Chan SW (2009) Photocatalytic reduction of chromium (VI) in aqueous solution using dye-sensitized nanoscale ZnO under visible light irradiation. *J Nanopart Res* 11(1):221
- Costa M, Klein CB (2006) Toxicity and carcinogenicity of chromium compounds in humans. *Crit Rev Toxicol* 36(2):155–163
- Katz SA, Salem H (1993) The toxicology of chromium with respect to its chemical speciation: a review. *J Appl Toxicol* 13(3):217–224
- Fazlzadeh M, Rahmani K, Zarei A, Abdoallahzadeh H, Nasiri F, Khosravi R (2017) A novel green synthesis of zero valent iron nanoparticles (NZVI) using three plant extracts and their efficient application for removal of Cr (VI) from aqueous solutions. *Adv Powder Technol* 28(1):122–130
- Li X, Ai L, Jiang J (2016) Nanoscale zerovalent iron decorated on graphene nanosheets for Cr (VI) removal from aqueous solution: surface corrosion retard induced the enhanced performance. *ChemEng J* 288:789–797
- Wu J, Wang XB, Zeng RJ (2017) Reactivity enhancement of iron sulfide nanoparticles stabilized by sodium alginate: Taking Cr (VI) removal as an example. *J Hazard Mater* 333:275–284
- Nasrollahzadeh M (2014) Green synthesis and catalytic properties of palladium nanoparticles for the direct reductive amination of aldehydes and hydrogenation of unsaturated ketones. *New J Chem* 38(11):5544–5550
- Lim SH, Radha B, Chan JY, Saifullah MS, Kulkarni GU, Ho GW (2013) Flexible palladium-based H₂ sensor with fast response and low leakage detection by nanoimprint lithography. *ACS Appl Mater Interfaces* 5(15):7274–7281
- Nasrollahzadeh M, Sajadi SM (2016a) Green synthesis of Pd nanoparticles mediated by *Euphorbia thymifolia* L. leaf extract: catalytic activity for cyanation of aryl iodides under ligand-free conditions. *J Colloid Interface Sci* 469:191–195
- Liu WJ, Ling L, Wang YY, He H, He YR, Yu HQ, Jiang H (2016) One-pot high yield synthesis of Ag nanoparticle-embedded biochar hybrid materials from waste biomass for catalytic Cr (VI) reduction. *Environ. Sci. Nano* 3(4):745–753
- Nasrollahzadeh M, Sajadi SM (2016b) Pd nanoparticles synthesized in situ with the use of *Euphorbia granulate* leaf extract: catalytic properties of the resulting particles. *J Colloid Interface Sci* 462:243–251
- Sheldon RA (2012) Fundamentals of green chemistry: efficiency in reaction design. *ChemSoc Rev* 41(4):1437–1451
- Nasrollahzadeh M, Sajadi SM, Babaei F, Maham M (2015) *Euphorbia helioscopia* Linn as a green source for synthesis of silver nanoparticles and their optical and catalytic properties. *J Colloid Interface Sci* 450:374–380
- Nasrollahzadeh M, Sajadi SM, Maham M, Kohsari I (2018) Biosynthesis, characterization and catalytic activity of the Pd/bentonite nanocomposite for base- and ligand-free oxidative hydroxylation of phenylboronic acid and reduction of chromium (VI) and nitro compounds. *Microporous Mesoporous Mater* 271:128–137
- Hazarika M, Borah D, Bora P, Silva AR, Das P (2017) Biogenic synthesis of palladium nanoparticles and their applications as catalyst and antimicrobial agent. *PLoS ONE* 12(9):e0184936
- Nasrollahzadeh M, Sajjadi M, Maham M, Sajadi SM, Barzinjy AA (2018) Biosynthesis of the palladium/sodium borosilicate nanocomposite using *Euphorbia milii* extract and evaluation of its catalytic activity in the reduction of chromium (VI), nitro compounds and organic dyes. *Mater Res Bull* 102:24–35
- Nasrollahzadeh M, Sajjadi M, Dadashi J, Ghafari H (2020) Pd-based nanoparticles: plant-assisted biosynthesis, characterization, mechanism, stability, catalytic and antimicrobial activities. *Adv Colloid Interface Sci* 276:102103
- Khodadadi B, Bordbar M, Nasrollahzadeh M (2017) *Achillea millefolium* L. extract mediated green synthesis of waste peach kernel shell supported silver nanoparticles: application of the nanoparticles for catalytic reduction of a variety of dyes in water. *J Colloid Interface Sci* 493:85–93
- Sureka J et al (2018) Synthesis of silver nano particle from *Gymnema sylvestre*: study of antimicrobial and antioxidant activity. *IJCRT* 6(1):897–902
- Gomathi M, Prakasam A, Rajkumar PV, Rajeshkumar S, Chandrasekaran R, Anbarasan PM (2020) Green synthesis of silver nanoparticles using *Gymnema sylvestre* leaf extract and evaluation of its antibacterial activity. *S Afr J ChemEng* 32:1–4
- Nakkala JR, Mata R, Bhagat E, Sadras SR (2015) Green synthesis of silver and gold nanoparticles from *Gymnema sylvestre* leaf extract: study of antioxidant and anticancer activities. *J Nanopart Res* 17(3):151
- Tiwari P, Mishra BN, Sangwan NS (2014) Phytochemical and pharmacological properties of *Gymnema sylvestre*: an important medicinal plant. *BioMed Res Int* 2014:1–18
- Arun LB, Arunachalam AM, Arunachalam KD, Annamalai SK, Kumar KA (2014) In vivo anti-ulcer, anti-stress, anti-allergic, and functional properties of Gymnemic acid Isolated from *Gymnema sylvestre* R Br. *BMC Complement Altern Med* 14(1):70
- Kanchana A, Devarajan S, Ayyappan SR (2010) Green synthesis and characterization of palladium nanoparticles and its conjugates from *Solanum trilobatum* leaf extract. *Nano Micro Lett* 2(3):169–176
- Kadam J, Dhawal P, Barve S, Kakodkar S (2020) Green synthesis of silver nanoparticles using cauliflower waste and their multifaceted applications in photocatalytic degradation of methylene blue dye and Hg²⁺ biosensing. *SN ApplSci* 2(4):1–16

28. Kora AJ, Rastogi L (2018) Green synthesis of palladium nanoparticles using gum ghatti (*Anogeissus latifolia*) and its application as an antioxidant and catalyst. *Arab J Chem* 11(7):1097–1106
29. Jangam K, Patil K, Balgude S, Patange S, More P (2021) Synthesis and characterization of magnetically separable $Zn_{1-x}Co_xFeMnO_4$ nanoferrites as highly efficient photocatalyst for degradation of dye under solar light irradiation. *J PhysChem Solids* 148:109700
30. Dewan A, Bharali P, Bora U, Thakur AJ (2016) Starch assisted palladium (0) nanoparticles as in situ generated catalysts for room temperature Suzuki–Miyaura reactions in water. *RSC Adv* 6(14):11758–11762
31. Kalaiselvi A, Roopan SM, Madhumitha G, Ramalingam C, Elango G (2015) Synthesis and characterization of palladium nanoparticles using *Catharanthus roseus* leaf extract and its application in the photo-catalytic degradation. *SpectrochimActa Part A MolBiomolSpectrosc* 135:116–119
32. Lakshmiopathy R, Reddy BP, Sarada NC, Chidambaram K, Pasha SK (2015) Watermelon rind-mediated green synthesis of noble palladium nanoparticles: catalytic application. *ApplNanosci* 5(2):223–228
33. Jin X, Liu Y, Tan J, Owens G, Chen Z (2018) Removal of Cr (VI) from aqueous solutions via reduction and absorption by green synthesized iron nanoparticles. *J Clean Prod* 176:929–936
34. Nasrollahzadeh M, Sajadi SM, Maham M (2015) Green synthesis of palladium nanoparticles using *Hippophae rhamnoides* Linn leaf extract and their catalytic activity for the Suzuki–Miyaura coupling in water. *J MolCatal A Chem* 396:297–303
35. Arunachalam KD, Arun LB, Annamalai SK, Arunachalam AM (2015) Potential anticancer properties of bioactive compounds of *Gymnema sylvestre* and its biofunctionalized silver nanoparticles. *Int J Nanomed* 10:31
36. Das RK, Borthakur BB, Bora U (2010) Green synthesis of gold nanoparticles using ethanolic leaf extract of *Centella asiatica*. *Mater Lett* 64:1445–1447
37. Sangeetha S, Archit R, SathiaVelu A (2014) Phytochemical testing, antioxidant activity, HPTLC and FTIR analysis of antidiabetic plants *Nigella sativa*, *Eugenia jambolana*, *Andrographis paniculata* and *Gymnema sylvestre*. *J Biotechnol* 9:1–9
38. Subashini MS, Rajendran P, Ashok G, Kanthesh BM (2015) TLC, FTIR and GCMS analysis of leaves of *Gymnema sylvestre* R. Br from Kolli Hills, Tamil Nadu, India. *Int J CurrMicrobiol App Sci* 4:757–764
39. Wang T, Lin J, Chen Z, Megharaj M, Naidu R (2014) Green synthesized iron nanoparticles by green tea and eucalyptus leaves extracts used for removal of nitrate in aqueous solution. *J Clean Prod* 83:413–419
40. Seku K, Hussaini SS, Golla N, Rapolu S, Bandi R, Reddy B (2020) Microwave-assisted synthesis of palladium nanoparticles using Frankincense resin and evaluation of their catalytic properties. *Mater Lett* 278:128427
41. Rathore B, Nazeruddin GM, PrasadKumbhar SRD, Khandare RV, Prasad N (2015) Extracellular one pot green synthesis of palladium nanoparticles. *Int J NanomaterNanostruct* 1:1–7
42. Celebi M, Yurderi M, Bulut A, Kaya M, Zahmakiran M (2016) Palladium nanoparticles supported on amine-functionalized SiO_2 for the catalytic hexavalent chromium reduction. *ApplCatal B* 180:53–64
43. Shi L-N, Zhang X, Chen Z-L (2011) Removal of Chromium (VI) from wastewater using 5 bentonite-supported nanoscale zero-valent iron. *Water Res* 45:886–892
44. Li S, Tang L, Zeng G, Wang J, Deng Y, Wang J, Zhou Y (2016) Catalytic reduction of hexavalent chromium by a novel nitrogen-functionalized magnetic ordered mesoporous carbon doped with Pd nanoparticles. *Environ SciPollut Res* 23(21):22027–22036
45. Tripathi RM, Rao RP, Tsuzuki T (2018) Green synthesis of sulfur nanoparticles and evaluation of their catalytic detoxification of hexavalent chromium in water. *RSC Adv* 8:36345–36352
46. Shao-feng N, Yong L, Xin-Hua XU, Zhang-hua L (2005) Removal of hexavalent chromium from aqueous solution by iron nanoparticles. *J Zhejiang UnivSci B* 6:1022–1027
47. Garole VJ, Choudhary BC, Tetgure SR, Garole DJ, Borse AU (2019) Palladium nanocatalyst: green synthesis, characterization, and catalytic application. *Int J Environ SciTechnol* 16(12):7885–7892
48. Ahmed MA, Elsir AT, Mohammed F, Elbushra HA, Tawer S, Eassa N (2018) Photo-reduction of chromium from water by TiO_2 nanoparticles. *MRS Advances* 3:2667–2674
49. Loryuenyong V, Jarunsak N, Chuangchai T, Buasri A (2014) The photocatalytic reduction of hexavalent chromium by controllable mesoporous anatase TiO_2 nanoparticles. *Adv Mater Sci Eng* 2014:1–8
50. Sanad MMS, Abdel-Aal EA, Osman HM, Kandil AT (2018) Photocatalytic reduction of hexavalent chromium with commercial Fe/Ti oxide catalyst under UV and visible light irradiation. *Int J Environ SciTechnol* 15(11):2459–2472
51. Tian X, Liu M, Iqbal K, Ye W, Chang Y (2020) Facile synthesis of nitrogen-doped carbon coated Fe_3O_4/Pd nanoparticles as a high-performance catalyst for Cr (VI) reduction. *J Alloys Compd* 826:154059
52. Guo Y, Zelekew OA, Sun, H, Kuo DH, Lin J, Chen X (2020) Catalytic reduction of organic and hexavalent chromium pollutants with highly active bimetal CUBiOS oxysulfide Catalyst under dark. *Sep Purif Technol* 116769
53. Liang M, Su R, Qi W, Zhang Y, Huang R, Yu Y, Wang L, He Z (2014) Reduction of hexavalent chromium using recyclable Pt/Pd nanoparticles immobilized on procyanidin-grafted eggshell membrane. *IndEngChem Res* 53:13635–13643
54. Huang Y, Ma H, Wang S, Shen M, Guo R, Cao X, Zhu M, Shi X (2012) Efficient catalytic reduction of hexavalent chromium using palladium nanoparticle-immobilized electrospun polymer nanofibers. *ACS Appl Mater Interfaces* 4:3054–3061
55. Li H, Gao M, Gao Q, Wang H, Han B, Xia K, Zhou C (2020) Palladium nanoparticles uniformly and firmly supported on hierarchical flower-like TiO_2 -nanospheres as a highly active and reusable catalyst for detoxification of Cr (VI)-contaminated water. *ApplNanosci* 10:359–369

Publisher's Note Springer Nature remains neutral with regard to jurisdictional claims in published maps and institutional affiliations.